



# RF CONTROL SYSTEM MODELING

Document date: June 28, 2007

Document contributors: Michel Luong, Olivier Piquet
CEA Saclay / DSM / DAPNIA / SACM

# 1 INTRODUCTION

On the roadmap to a fault tolerant ADS for radioactive waste transmutation, the simulation and prediction of the proton linac behaviour accounting for the performance of the RF control system have been identified as an essential task since they form the baseline strategy for the fast recovery of the nominal proton beam energy and power in case of failure due to any critical component of the linac. A superconducting cavity quench can be considered the most severe failure that the RF control of all the other cavities should be able to cope with. The main characteristics and requirements for such an RF control system were presented in a previous deliverable [1]. Obviously, a system modeling must be addressed in order to allow reliable simulations. However, the physical phenomena and perturbations involved in an RF accelerating cavity for protons come under such a high complexity that the simulation models and parameters should be refined as the design and analysis of the different components progress. This attitude appears all the more necessary as regards Lorentz force detuning, microphonics and their compensation by means of piezoelectric tuner. Therefore, the modeling discussed in this document should be considered only as one possible approach the advantages and limitations of which will be pointed out.

The modeling of the accelerating cavity and its interaction with the proton beam will be an extension of the one used for relativistic electron beam based on the concept of shunt impedance and on the representation of generator, cavity, and beam induced voltages with phasors. Provided that some precautions are taken in the computations of the shunt impedance and synchronous phase, this model still gives a very good approximation to compute the beam loading and the energy gain for a cavity driven by a feedback control system. This representation forms a backbone for the system simulation. Implemented with a Matlab/Simulink [2], it allows all kinds of system customization and analysis in a very flexible way. For instance, the effect of the analogue to digital converter resolution or the generator power limitation could be assessed using the dedicated Simulink blocks.

When a cavity is detuned from the generator frequency which is defined as the reference frequency, the cavity voltage amplitude and phase are affected, resulting in an energy gain deviation for one proton bunch from its nominal value. This means a different beam loading and the next bunch will see a cavity phasor disrupted first by the detuning and secondly by the modified beam loading. The series of perturbation propagate along the bunches until a new equilibrium is established if any other detuning has not occurred and if the cavity voltage does not change the detuning in return. In practice, such a feedback process does exist in superconducting cavities made up of a thin niobium wall due to electromagnetic pressure, effect known as Lorentz force detuning. The dynamic coupling of these phenomena may lead to an amplification effect producing unacceptable beam loss in a linear accelerator. The initial detuning may be imparted by mechanical vibrations usually called microphonics or by the coupling of beam loading to the Lorentz force detuning itself in the case of a chopped beam. The RF control system is designed to maintain the cavity voltage phasor constant in order to provide the same energy gain to any bunch. The RF control system modeling is an attempt to simulate such a multi-loops system to predict the beam energy spread at the output of one cavity or at the output of an entire linac.

# 2 ACCELERATING PROTONS WITH AN RF CAVITY

For an electron whose rest mass is 1836 times lower compared to the proton rest mass, its velocity grows quickly as energy is gained. It reaches already 90% of the speed of light at a kinetic energy of 1 MeV. In a high energy linac, the velocity of the electrons that compose a bunch can be considered constant. This feature represents a great simplification while dealing with the acceleration of electrons in a RF cavity, and a well proven model was elaborated a dozens of years ago [3]. On the contrary, protons velocity does not exceed 50% of speed of light even at energy higher than 100 MeV. The fact that the velocity of the particles can change according to their energy is generally referred as phase slippage. It occurs inside and outside of a cavity for particle bunches having different energies. The phase slippage is the underlying process which causes the maximum energy gain in a standing wave cavity to depend on the energy at the cavity input, and also the shunt impedance to be no longer a parameter independent to the beam energy and phase at the input of a cavity. In the present discussion, only standing wave cavities are concerned. Even if the modeling approach may be extended to the case of travelling wave structure, its discussion is out of the scope of this report since none of such structures is under consideration for the Eurotrans project.

## 2.1 Standing wave elliptical five-cell cavity

To illustrate the modeling approach, a five-cell elliptical cavity [4] operating at 704.4 MHz designed for a geometrical beta, $\beta_g = 0.47$ has been chosen. This parameter is defined by: $\beta_g=2Lf_0/c$, where $L$, $f_0$, and $c$ stand respectively for the physical length of one cell, the operating frequency, and the speed of light. With this definition which is the one generally adopted by the cavity designer, a cavity of a given beta does not mean necessarily that the energy gain is optimized for protons entering the cavity with the same relativistic beta, ratio of $v/c$. For the energy gain and cavity model parameters computations, a normalized profile $p(z)$ of the longitudinal component of the electric field $E_z$ on the cavity axis is needed. It is obtained from a numerical simulation of the cavity with the Ansoft HFSS code and includes two short sections of the beam pipe in order to take into account the evanescent field. Then $E_{z0}(z) = G\, p(z)$ where $G$ is limited by the critical magnetic field of the superconductor or by field emission. For this cavity, $G$ should not exceed 28.5 MV/m corresponding to a maximum surface field of 50 MV/m.

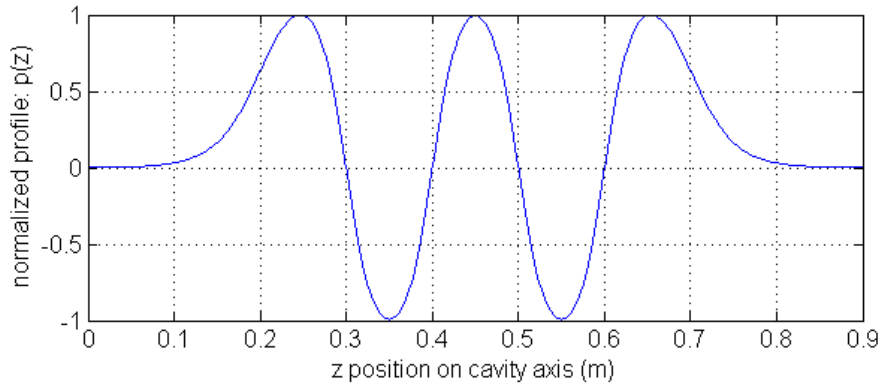


Figure 1: Normalized profile of $E_z$ for the elliptical five-cell cavity.

## 2.2 Energy gain computation

The energy gain for a proton across the cavity is obtained by integrating in the time domain the differential equation that describes the longitudinal motion accounting for the relativistic effect:

$$\ddot{z} = \left(1 - \frac{\dot{z}^2}{c^2}\right)^{3/2} \frac{q\,E_z(z,t)}{m}, \tag{1}$$

with an initial velocity $v_0$ given by the particle kinetic energy $\xi$ at the cavity input ($z = 0$), and $E_z(z,t) = E_{z0}(z)\cos(\omega t + \phi_0)$ the time varying accelerating field where $\phi_0$ is the RF phase when the particle enters the cavity; this is a phase that can be measured from the cavity pickup signal. Parameters $q$ and $m$ represent the charge and the rest mass of the particle. Denoting $k = \xi / mc^2$, the link between $v_0$ and $\xi$ writes:

$$v_0 = c\sqrt{1 - \frac{1}{(1+k)^2}}\,. \tag{2}$$

The differential equation Eq. (1) is solved numerically using the Runge-Kutta method with Simulink as shown in Figure 2. A time step of 10 ps ensures a relative energy gain accuracy better than 2 $10^{-8}$. This tracking process also provides the velocity distribution or beta distribution along the cavity axis necessary to the calculation of the cavity voltage synchronous phase a shunt impedance discussed in the following section.

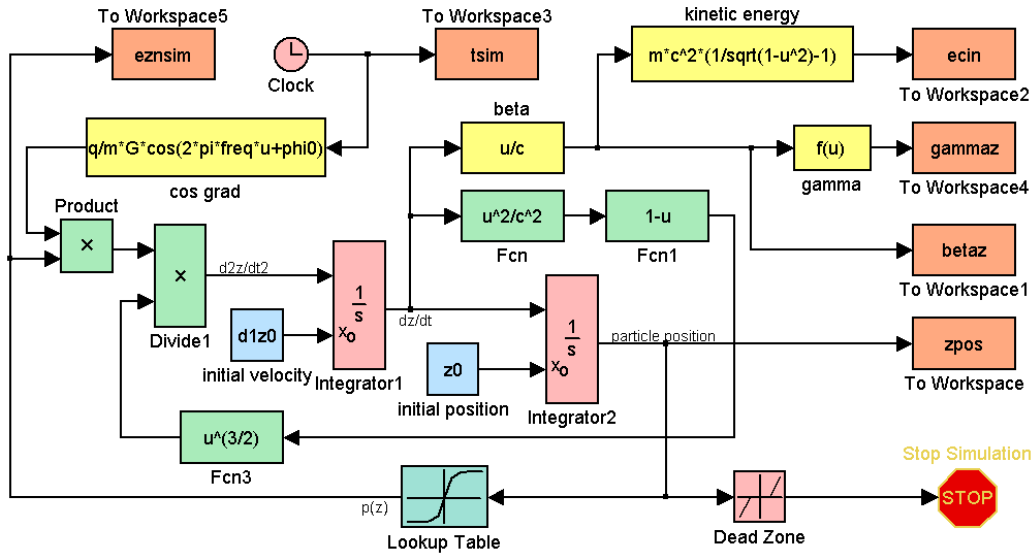


Figure 2: Energy gain computation scheme in Simulink.

In order to show how the maximum energy gain changes according to the initial energy, and gradient $G$ of 20 MV/m has been considered with a 30% safety margin to maximum gradient set by the field emission. It appears that the maximum gain is not reached when the particle has a velocity corresponding to a relativistic beta equal to the geometric beta (Figure 2). In this case, the optimum beta is found around 0.52, i.e. for an initial energy of 160 MeV compared to a geometric beta of 0.47 for 124 MeV.

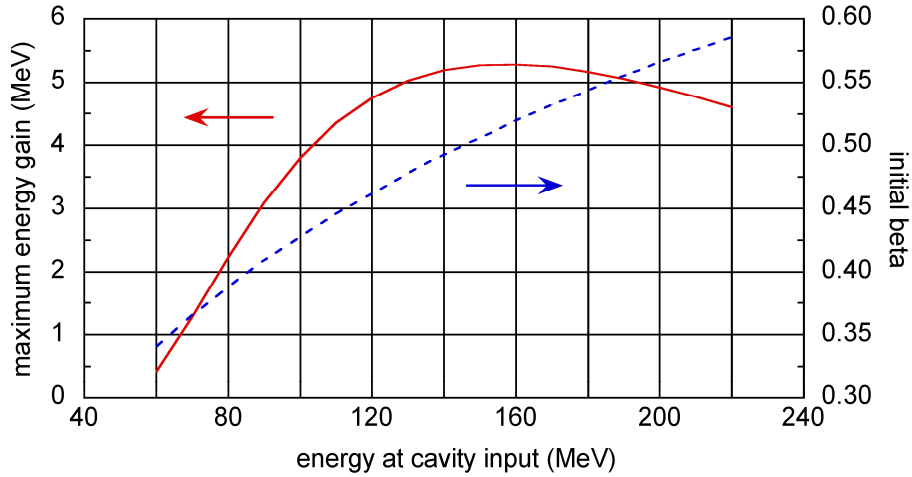


Figure 3: Maximum energy gain versus initial energy ($G$ = 20 MV/m).

The tracking code also provides the gain profile and phase slippage inside the cavity (Figure 4). An example is given for a particle with input energy of 124 MeV corresponding to a beta of 0.47. The phase slippage, defined as: $\omega$ (*tsim-zpos*/0.47*c*), where the variables involved are those that appear in Figure 2, relates the phase difference between the particle being accelerated and a virtual reference particle travelling across the cavity without velocity change. A negative value means phase advance while positive value means phase lag. However, the phase slippage does not represent an issue in a linac but only a phase offset when all bunches experience the same acceleration. It can be easily compensated from one cavity to the next.

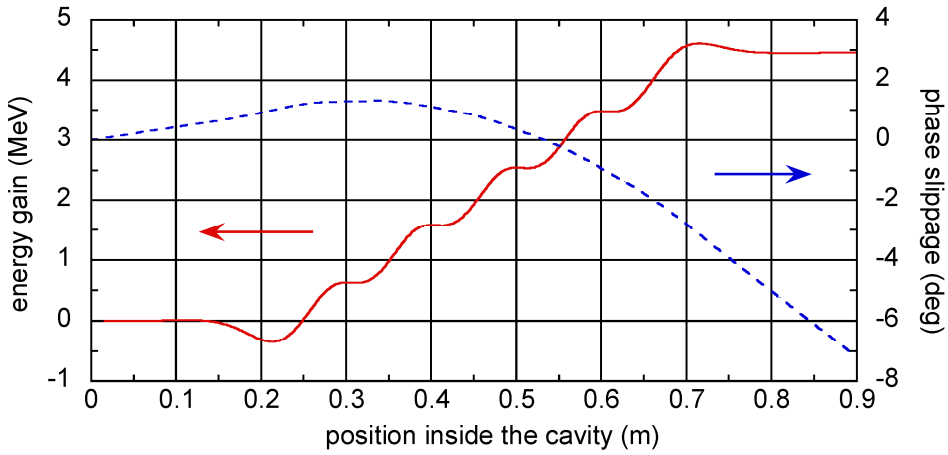


Figure 4: Energy gain and phase slippage inside a cavity (entering particle: $\beta = 0.47$).

## 2.3 Cavity model and shunt impedance

Thes present study adopted a model widely used for high energy linac. It is based on one hand on the calculation of a cavity voltage phasor $\tilde{V}_{cav}$ from which the energy gain can be derived, and on the other hand on the calculation of a shunt impedance $R_s$ that makes the analysis of the whole RF system very convenient using a RLC equivalent circuit [3]. The amplitude $V_{cav}$ and phase $\phi_s$, also called synchronous phase of $\tilde{V}_{cav}$ are computed in the case of a relativistic particle i.e. $\beta \approx 1$ by a direct integration of the cavity $E_z$ profile (Figure 1):

$$V_{cav} = \sqrt{a^2 + b^2},\ \tan\phi_s = \frac{b}{a}, \qquad \text{defining} \quad \tilde{V}_{cav} = V_{cav}\exp(\mathrm{j}\phi_s), \tag{3}$$

$$a = \int_0^{z\max} E_z(z)\cos\left(\omega\frac{z}{c} + \phi_0\right)dz,\ b = \int_0^{z\max} E_z(z)\sin\left(\omega\frac{z}{c} + \phi_0\right)dz. \tag{4}$$

Then, the ratio of shunt impedance to the quality factor $R_s/Q$ is obtained after normalization to the stored energy $W_{stored}$ corresponding to the $E_z$ profile:

$$\frac{R_s}{Q} = \frac{V_{cav}^2}{2\omega W_{stored}}. \tag{5}$$

In that case, it can be shown that the factor of merit $R_s/Q$ is gradient $G$ independent. Furthermore, $\phi_s$ and $\phi_0$ only differ from one constant phase offset, and the energy gain writes: $\Delta\xi = \mathrm{Re}(\tilde{V}_{cav}) = V_{cav}\cos\phi_s$. The synchronous phase is nothing else than the phase shift between the cavity voltage and the beam considered as a reference.

In the case of a heavy particle whose velocity increases slowly as energy is gained, equations Eq. (4) should be modified consequently [5] providing an extension of the former model:

$$a = \int_0^{z\max} E_z(z)\cos\phi(z)dz,\ b = \int_0^{z\max} E_z(z)\sin\phi(z)dz, \tag{6}$$

$$\text{with} \qquad \phi(z) = \frac{\omega}{c}\int_0^z \frac{dz'}{\beta(z')} + \phi_0.$$

It should be reminded that the $\beta(z)$ distribution is the one obtained with a particle tracking while applying a cosine time dependant gradient. When the particle tracking is performed in the time domain, equation Eq. (6) is implemented in Matlab, referring to the variable names defined in Figure 2, as:

$$a = \mathrm{trapz}(zpos,\ G*\ eznsim.*\cos(2*\mathrm{pi}*freq*tsim+phi0)), \tag{7}$$

$$b = \mathrm{trapz}(zpos,\ G*eznsim.*\sin(2*\mathrm{pi}*freq*tsim+phi0)).$$

Now, contrary to the constant velocity case, the value of $R_s/Q$ and the phase shift between synchronous phase and RF phase are no more constant. The deviation of the latter can be seen while plotting the quantity $\phi_s$-$\phi_0$-mean($\phi_s$-$\phi_0$) against $\phi_0$. As another consequence, the variation of the energy gain as a function of the RF phase also deviates from a cosine function, and seems to question the very foundation of the voltage phasor concept. These deviations are all the more significant as the input energy is low and the accelerating gradient is high. An illustration of these effects are shown on Figure 5 for an input energy of 80 MeV and $G$ = 20 MV/m. It can be noticed that, fortunately the deviations are minimum in the vicinity of maximum gain. In the perspective of RF control system simulation where only small excursions from a nominal setting are considered, the phasor model can still be used with a good enough approximation. It also appears that the maximum energy gain does not correspond to a zero synchronous phase; a discrepancy up to tens degrees can be observed for very low input energy because $V_{cav}$ is not constant even for a given input energy and gradient. The $V_{cav}$ variation results directly in a variation of $R_s/Q$ because of Eq. (5).

Unlike the electron cavity, a proton cavity shows also a very strong dependency to the input energy of the particles (Figure 6). For high gradient, the particle velocity change inside the cavity leads to dependency to RF phase, i.e. to the synchronous phase that may rise to a

few tens percent. Consequently, for each physically identical cavity in a linac, the $R_s/Q$ factor should be computed for a given energy gain, synchronous phase, and input energy, using a tracking code as shown in Figure 2. A proton cavity in a linac will be modeled with a set of $V_{cav}$, $R_s/Q$, and $\phi_s$. For example, a cavity that has to provide an energy gain of 4 MeV to protons with an input energy of 124.7 MeV i.e. $\beta$=0.47, and a designed synchronous phase of -25° ($\phi_0$ = -113.5°) would be characterized in the cavity model by: $V_{cav}$ = 4.413 MV, $R_s/Q$ = 84.39 Ω. The corresponding gradient $G$ is 18.083 MV/m. These parameters are considered as nominal for the all developments in the following sections.

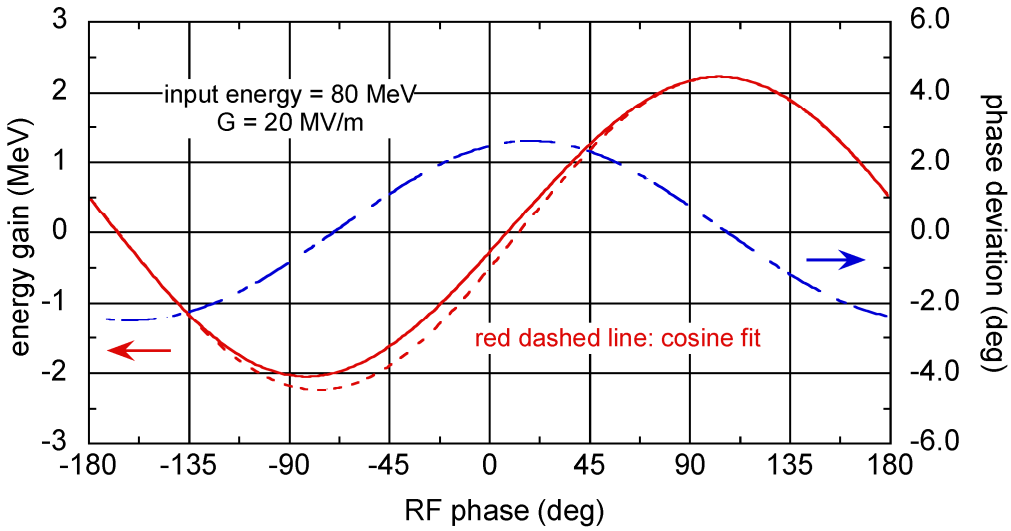


Figure 5: Cavity voltage phasor model consistency evaluation.

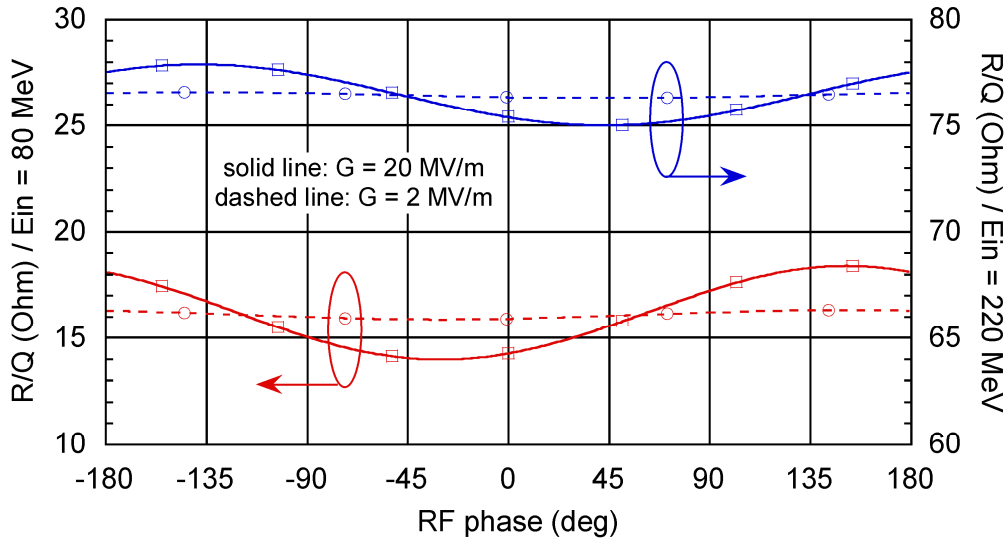


Figure 6: $R_s/Q$ as function of input energy, gradient and RF phase.

## 2.4 Correction for injection energy error

In addition to the $R_s/Q$, the synchronous phase and the exit phase are also significantly dependent on the input energy. The exit phase is defined from the time when the particle has crossed the cavity compared to the particle with the nominal energy: $\phi_e(\xi) = \omega[t_{out}(\xi)-t_{out}(\xi_0)]$. Thus, the exit phase is zero for a particle with no energy error. Fortunately, RF control system

analysis only needs to deal with very small energy deviation since the energy acceptance of a proton linac is usually limited to less than 1%. Therefore, a first order expansion of these parameters as function of input energy will provide a good approximation:

$$\begin{aligned} \frac{R_s}{Q}(\xi) &= \frac{R_s}{Q}(\xi_0) + \frac{\partial R_s/Q}{\partial \xi}\mathrm{d}\xi, \\ \phi_s(\xi) &= \phi_s(\xi_0) + \frac{\partial \phi_s}{\partial \xi}\mathrm{d}\xi \\ \phi_e(\xi) &= \frac{\partial \phi_e}{\partial \xi}\mathrm{d}\xi \end{aligned} \tag{8}$$

The first derivatives are computed numerically using the energy tracking code. Table 1 gives the numerical values of the relevant parameters for an energy deviation of ±1%. The linear correction factor for $R_s/Q$, $\phi_s$ and $\phi_e$ are respectively: 0.962 Ω/MeV, −2.60°/MeV, and −4.88°/MeV.

Table 1 – Cavity parameters variation on input energy small errors

| input energy (MeV) | $R_s/Q$ (Ohm) | $\phi_s$ (°) | $t_{out}$ (ns) | $\phi_e$ (°) |
|---|---|---|---|---|
| $\xi_0$ = 124.7 | 84.389 | -25.00 | 6.349 | 0 |
| 0.99 $\xi_0$ | 83.134 | -21.68 | 6.374 | 6.34 |
| 1.01 $\xi_0$ | 85.589 | -28.25 | 6.325 | -6.09 |

Finally, the cavity model used for constant velocity beam can be extended to velocity varying beam with a good approximation in regard to the cavity RF control simulation provided that $V_{cav}$ and $R_s/Q$ are computed carefully using a tracking code. A definite advantage of this model choice is that all the formalism developed for high energy electron cavity simulation [3,6,7,8] can be directly transposed to the proton cavity. Furthermore, this model allows a very flexible implementation using Matlab/Simulink with minimum memory and simulation time.

# 3 RF CONTROL SYSTEM MODELING

The simulation of an RF control system consists in solving numerically a set of coupled differential equations describing the dynamic behaviour of the cavity, beam loading, feedback loop and perturbations. There are many alternatives to formulate these equations. The cavity voltage phasor can be seen as a doublet of amplitude and phase, or of in-phase and quadrature phase components. The latter convention was chosen in this document. Particle beam may be represented with a current, i.e. a single variable in the simulation, or with a succession of bunches characterized by an energy and a phase. The first method allows a faster simulation which produces the necessary information as long as a single cavity is concerned. The second method is suited for analysis of the longitudinal stability of a linac composed of a succession of cavities and requires longer simulation time and memory resource. Many perturbations sources model can be easily inserted in the simulation carried out with Matlab and Simulink. This report will only focus on the major perturbations known as microphonics and Lorentz force detuning, and their possible compensation with a piezoelectric tuner.

## 3.1 Cavity equations

Denoting $Q_L$ the loaded quality factor of the cavity, $\boldsymbol{V_c}$ the cavity voltage, $\omega_0$ the resonant angular frequency, and $\boldsymbol{I_g}$ the generator current, the equivalent RLC model provides a differential equation characteristic of a cavity driven by a current generator in the absence of any beam:

$$\frac{d^2\boldsymbol{V}_c}{dt^2}+\frac{\omega_0}{Q_L}\frac{d\boldsymbol{V}_c}{dt}+\omega_0^2\boldsymbol{V}_c=\frac{\omega_0 R_L}{Q_L}\frac{d\boldsymbol{I}_g}{dt}, \tag{9}$$

where $R_L$ is resistor seen on the cavity side. While defining $\beta_{RF}$ as the coupling of the transmission line to the cavity, $R_L$ writes:

$$R_L=\frac{R_s}{1+\beta_{RF}}=\left(\frac{R_s}{Q}\right)Q_L. \tag{10}$$

In sinusoidal regime, $\boldsymbol{V}_c=\tilde{V}_c\exp(j\omega t)$, and $\boldsymbol{I}_g=\tilde{I}_g\exp(j\omega t)$. Replacing these expressions in Eq. (9) and neglecting the second order derivative, which conveys a very good approximation for resonant cavity with a filling time much higher the RF period, an equation is obtained for the phasors $\tilde{V}_c$ and $\tilde{I}_g$ :

$$\tau\frac{d\tilde{V}_c}{dt}+(1+j\,y)\,\tilde{V}_c=R_L\tilde{I}_g,\ \text{with}\ \tau=\frac{2Q_L}{\omega_0}\ \text{and}\ y=-\tan\psi\approx 2Q_L\frac{\omega-\omega_0}{\omega_0}. \tag{11}$$

The variable $\psi$ is called the detuning angle. With a feedback loop, $\tilde{I}_g=\tilde{I}_{g0}+K\left(\tilde{V}_{c0}-\tilde{V}_c\right)/R_L$, where $K$ is the open loop gain. Then, expanding the phasor into real and imaginary part denoted with subscript $r$ and $i$, a set of two coupled differential equations is obtained:

$$\begin{aligned}\tau\frac{dV_{cr}}{dt}+V_{cr}-yV_{ci}&=R_L I_{g0r}+K\left(V_{c0r}-V_{cr}\right),\\ \tau\frac{dV_{ci}}{dt}+V_{ci}+yV_{cr}&=R_L I_{g0i}+K\left(V_{c0i}-V_{ci}\right).\end{aligned} \tag{12}$$

For a beam characterized by $q_b$ the charge per bunch and $T_b$ the bunch separation period, a mean current $I_0 = q_b/T_b$ is derived. It can be shown [3] that a reactive compensation of the beam loading is obtained by a proper detuning of the cavity. It means that the generator current and the cavity voltage have the same phase which can be taken as the zero reference phase, i.e. $I_{g0i} = V_{c0i} = 0$. Then, denoting $V_{c0r} = V_{cav}$ and $I_{g0r} = I_{g0}$, equations Eq. (12) simplify to:

$$\begin{aligned}\tau\frac{dV_{cr}}{dt}+V_{cr}-yV_{ci}&=R_L I_{g0}+K\left(V_{cav}-V_{cr}\right),\\ \tau\frac{dV_{ci}}{dt}+V_{ci}+yV_{cr}&=-KV_{ci}.\end{aligned} \tag{13}$$

The reactive compensation is obtained under the condition:

$$\tan\psi=\frac{2I_0R_L}{V_{cav}}\sin\phi_s, \tag{14}$$

with a synchronous phase defined as negative. Till now, the beam loading has not been

described, and only the generator current is considered in Eq. (13). Since the travelling time of a bunch across a cavity is very short compared to the filling time, the beam loading action may be seen as an instantaneous effect. The cavity voltage just after the crossing of a bunch is given by the beam loading theorem [3]:

$$\begin{aligned} V_{cr}^{+} &= V_{cr} - \omega \frac{R_s}{Q}(\xi)\, q_b \cos\left[\phi_s(\xi) + \phi_c + \Delta\phi_b\right], \\ V_{ci}^{+} &= V_{ci} - \omega \frac{R_s}{Q}(\xi)\, q_b \sin\left[\phi_s(\xi) + \phi_c + \Delta\phi_b\right]. \end{aligned} \tag{15}$$

with $\tan \phi_c = V_{ci}/V_{cr}$ and $\Delta\phi_b = \phi_{inj}$ if the cavity is the first cavity or $\Delta\phi_b = \phi_e + \phi_d$ otherwise. The variables $\phi_{inj}$, $\phi_e$ and $\phi_d$ stand respectively for the injection phase error, the exit phase at the upstream cavity and $\phi_d$ the phase slippage in the drift section before the simulated cavity due to the error in energy gain. Now from Eq. (15), it appears clearly that the energy and phase error of each bunch should be known along a linac. Thus, denoting the reference to the $n^{th}$ cavity with a superscript and letting $\xi^{n,k}$ and $\Delta\phi_b^{n,k}$ be respectively the energy of a bunch $k$ at the entrance of the $n^{th}$ cavity and its phase error referred to the nominal phase, each cavity preceded by a drift section of length $L^n$ upstream, their variation cavity after cavity is described by the equations:

$$\begin{aligned} \xi^{n+1,k} &= \xi^{n,k} + \Omega^{n,k} \left| V_{cr}^{n} + jV_{ci}^{n} \right| \cos\left[\phi_s^{n,k} + \phi_c^{n} + \Delta\phi_b^{n,k}\right], \\ \Delta\phi_b^{n+1,k} &= \Delta\phi_b^{n,k} + \phi_e^{n,k} + \phi_d^{n,k}, \\ \Omega^{n,k} &= \left.\frac{R_s}{Q}\right|^{n,k} \Big/ \left.\frac{R_s}{Q}\right|_0^{n}, \\ \left.\frac{R_s}{Q}\right|^{n,k} &= \left.\frac{R_s}{Q}\right|_0^{n} + \frac{\partial}{\partial\xi}\left(\left.\frac{R_s}{Q}\right|^{n}\right)_{\xi_0^n} \left(\xi^{n,k} - \xi_0^n\right), \\ \phi_s^{n,k} &= \phi_{s0}^{n} + \frac{\partial}{\partial\xi}\left(\phi_s^n\right)_{\xi_0^n} \left(\xi^{n,k} - \xi_0^n\right), \\ \phi_e^{n,k} &= \frac{\partial}{\partial\xi}\left(\phi_e^n\right)_{\xi_0^n} \left(\xi^{n,k} - \xi_0^n\right), \\ \phi_d^{n,k} &= \omega L^n \left(\frac{1}{v^{n,k}} - \frac{1}{v_0^n}\right) \approx -\omega L^n \frac{v^{n,k} - v_0^n}{\left(v_0^n\right)^2}, \\ v^{n,k} &= c\sqrt{1 - \frac{1}{(1 + \xi^{n,k}/mc^2)^2}}, \\ V_{cr}^{n+} &= V_{cr}^{n} - \omega \left.\frac{R_s}{Q}\right|^{n,k} q_b^k \cos\left[\phi_s^{n,k} + \phi_c^{n} + \Delta\phi_b^{n,k}\right], \\ V_{ci}^{n+} &= V_{ci}^{n} - \omega \left.\frac{R_s}{Q}\right|^{n} q_b^k \sin\left[\phi_s^{n,k} + \phi_c^{n} + \Delta\phi_b^{n,k}\right]. \end{aligned} \tag{16}$$

The subscript zero in the previous set of equations refers to the nominal value. Furthermore, it easy to realize that $\xi^1$ and $\Delta\phi_b^1$ represent the energy and error of phase at injection and $\phi_d^1$ is null if there is no drift section between the first cavity and the place where the injection

energy is measured. All the equations given above form the baseline for an RF control system simulation in the absence of any perturbation.

The nominal generator power required for the cavity operation without perturbation is given by the following equation:

$$P_{g0} = \frac{1+\beta_{RF}}{\beta_{RF}} \frac{V_{cav}^2}{8R_L} \left\{ \left[ \frac{\cos\phi_s}{\cos\psi} + \frac{2I_0R_L}{V_{cav}} \cos\psi \right]^2 + \left[ -\frac{\sin\phi_s}{\cos\psi} + \frac{2I_0R_L}{V_{cav}} \sin\psi \right]^2 \right\}, \tag{17}$$

reminding that $\phi_s$ is defined negative. For superconducting cavity, $\beta_{RF} >> 1$ and if the condition of reactive compensation in Eq. (14) is satisfied, equation Eq. (17) simplifies to:

$$P_{g0} \approx \frac{1}{8R_L} \left( V_{cav} + 2I_0R_L \cos\phi_s \right)^2, \tag{18}$$

and the nominal generator current is given by:

$$I_{g0} \approx \sqrt{8P_{g0}/R_L}\,. \tag{19}$$

Application of equations Eq. (11), (14), (17), (18) and (19) lead to the nominal parameters related to the power consideration. They are summarized in Table 2. The left part of the table reminds of the cavity parameters used as inputs for the calculation.

Table 2 – Nominal power parameters

| | | | |
|---|---|---|---|
| $\omega_0/2\pi$ (MHz) | 704.4 | $\tan\psi$ | -0.404 |
| $I_0$ (mA) | 5 | $\psi$ (°) | -22 |
| $V_{cav}$ (MV) | 4.413 | $(\omega-\omega_0)/2\pi$ (Hz) | 28.4 |
| $\phi_s$ (°) | -25 | $P_{g0}$ (kW) | 20.1 |
| $R_s/Q$ (Ohm) | 84.39 | $I_{g0}$ (mA) | 19.5 |
| $Q_L$ | $5\ 10^6$ | $V_{g0}$ (MV) | 8.23 |

In closed loop operation, perturbations compensation requires an extra power. $P_g$ is then calculated using $\left|\tilde{I}_g\right| = \left|\tilde{I}_{g0} + K\left(\tilde{V}_{c0} - \tilde{V}_c\right)/R_L\right|$ instead of $I_{g0}$ in Eq. (19).

## 3.2 Perturbations

Superconducting cavities made up of thin niobium wall are subjected to mechanical deformations due to external forces like the liquid helium bath pressure or structure resonances. As a result, the cavity is dynamically detuned. This perturbation is usually designated as microphonics. The lower the resonance frequency, the stronger the perturbation. The overall effect may not be easily modeled in details because of many possible external excitation sources. Furthermore, the latter are strongly dependent on the environment. However, it is possible to measure the detuning as a function of time in situ using a phase demodulation setup as shown on Figure 7. Then, the recorded detuning may be used in simulation assuming that it is externally and independently imposed. Otherwise, the detuning may also be mathematically described as a sum of slowly modulated harmonic oscillations:

$$\Delta\omega_\mu(t) = \sum_i^N \overline{\Delta\omega_i}(t) \sin\left(\omega_i t + \varphi_i\right). \tag{20}$$

This general formulation allows the description of the mechanical resonance with eigenfrequency $\omega_i$, which can be identified by a Fourier analysis of the recorded detuning signal (Figure 8, Figure 9). More details are found in [9].

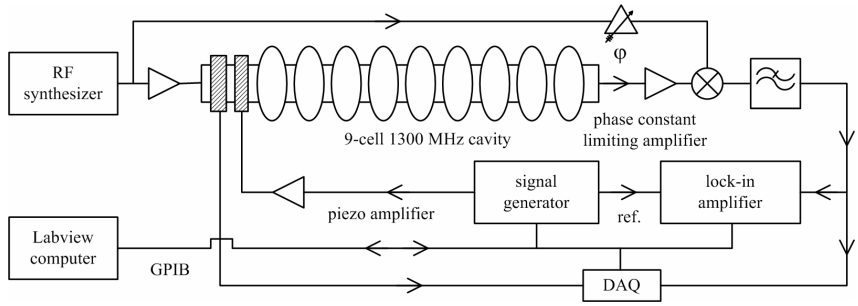


Figure 7: Experimental setup for microphonics and transfer function analysis.

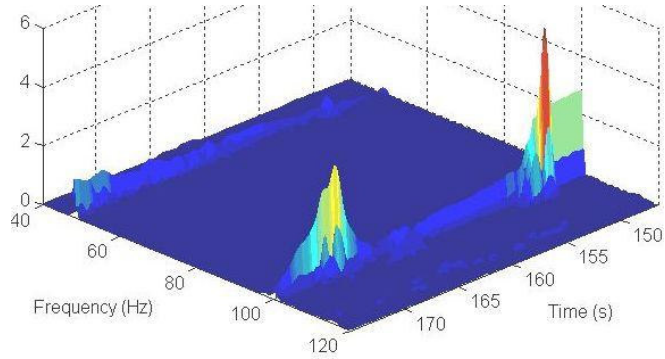


Figure 8: Spectrogram of vacuum pumps motors harmonics driven microphonics.

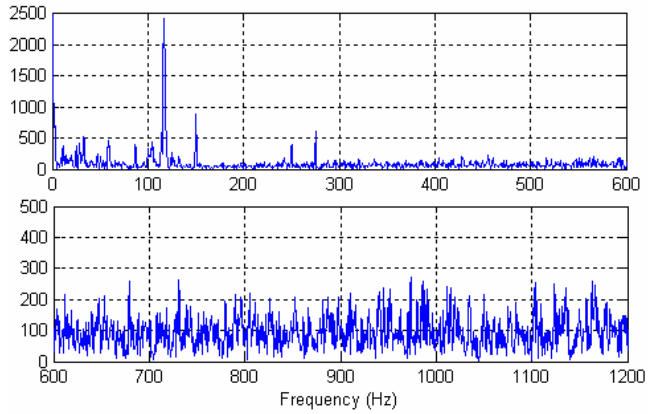


Figure 9: Spectrum of microphonics due to other environmental noises.

In an RF cavity, the standing electromagnetic wave induces surface currents on the cavity wall in the presence a high magnetic field and gives rise to the Lorentz force or pressure, which is proportional to the square of the accelerating gradient. Under the Lorentz pressure, the cavity takes a new shape, which can be seen as the superposition of a high number of eigenmodes or mechanical modes (Figure 10). The contribution of each mode to the cavity detuning is governed by a second order differential equation:

$$\frac{d^2\Delta\omega_m}{dt^2}+\frac{\omega_m}{Q_m}\frac{d\Delta\omega_m}{dt}+\omega_m^2\Delta\omega_m=-2\pi k_m\omega_m^2E_{acc}^2\,, \tag{21}$$

where $E_{acc}$ is the ratio of $V_{cav}$ to the cavity length. The parameters $\omega_m$, $Q_m$ and $k_m$ of the equation may be measured with a setup similar to the one presented in Figure 7 where the

signal generator is used to modulate the amplitude of the RF synthesizer signal. For small modulation, the Lorentz pressure is proportional to the modulating voltage. Except the mechanical quality factor, the eigen-frequency $\omega_m$ and Lorentz detuning sensitivity $k_m$ can also be computed numerically [10]. However, the results may differ from the experimental values because the mechanical boundary conditions can not be modeled with precision. But they provide a rough estimation, which is usually enough for RF system simulation.

The total detuning on the cavity is the sum of all contributions:

$$\Delta\omega_L(t) = \sum_{m=1}^{N} \Delta\omega_m(t) \tag{22}$$

In steady state, the total detuning sensitivity is nothing than the sum of $k_m$. Using the 55 km values computed for the medium β cavity, this sum gives 1.65 Hz/(MV/m)$^2$, which is to be compared 1.7 Hz/(MV/m)$^2$, the coefficient given by static detuning calculation. This indicates that a sufficient number of modes have been taken into account in order to reproduce the static behaviour successfully.

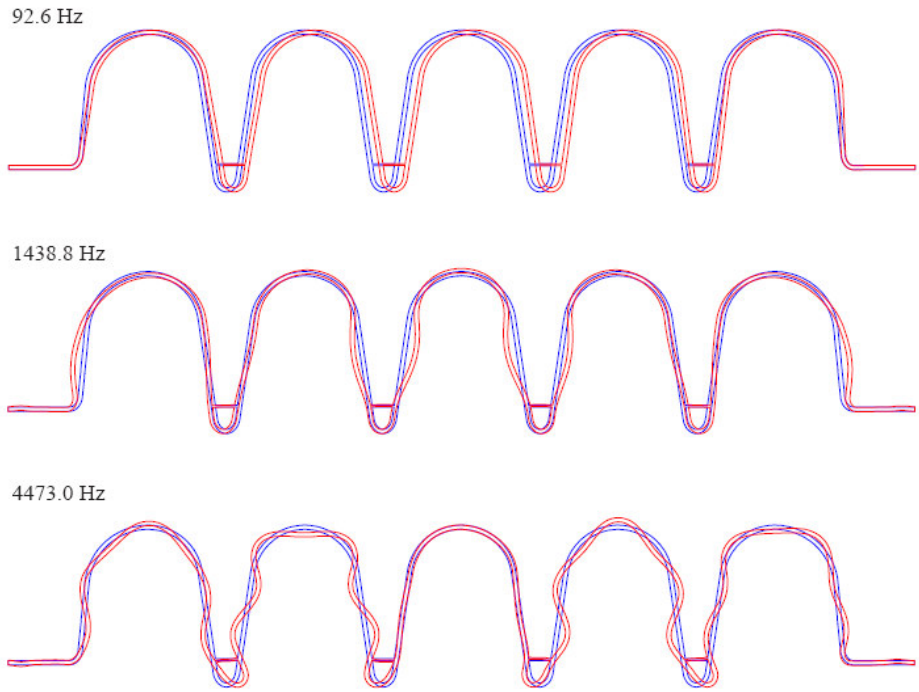


Figure 10: Three mechanical modes (red: magnified deformation).

A detuning of a cavity whatever it is due to the microphonics or Lorentz force generate a request for additional power, which can or can not be satisfied by the power source budget. As an example, if one considers a cavity with the parameters shown in Table 2, which has a total bandwidth of 140 Hz, a 35 Hz amplitude detuning would require an extra power of about 7% from Eq. (17). This extra power climbs by 28% for a 70 Hz amplitude detuning. Actually, it scales as the square of the detuning. Since additional power means additional cost, it may be very attractive to try and compensate the detuning perturbation by a fast piezo tuner (FPT), the response time of which should be lower than 1 ms. The low power dissipation of piezoelectric actuators represent the most promising solution of fast tuner implementation for superconducting cavities.

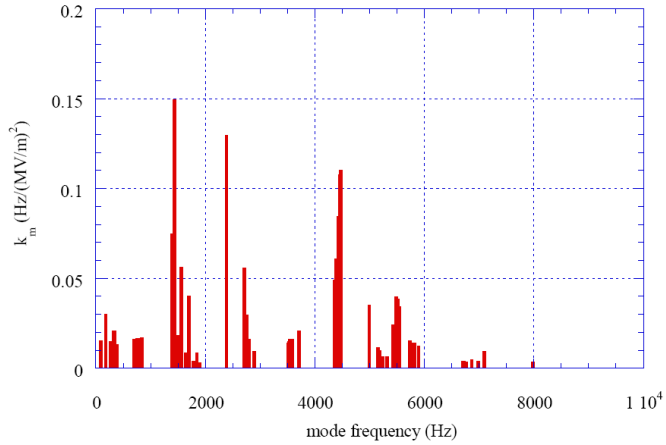


Figure 11: Eigen-frequencies and Lorentz detuning sensitivity (first 55 modes).

Assuming a linear response for a fast tuner, the measure of the transfer function (TF), i.e. amplitude and phase response for harmonic excitation (Figure 7) provides a full description of the system. Figure 12 shows an example of transfer function measured on a fast tuner designed for a 1.3 GHz 9-cell cavity, which should not differ significantly to the one that could be measured on a 5-cell cavity. Again, the resonances identifiable in the transfer function correspond to the mechanical resonance of the cavity. An analytical model can be derived from the transfer function [9]. The mathematical formulation is reminded below:

$$H(s) = H^1(s) + \sum_{i=1}^{N} H_i^2(s), \quad H^1(s) = \frac{K_0}{\tau s + 1},$$
$$H_i^2(s) = \frac{\omega_i^2 K_i}{s^2 + 2\zeta_i \omega_i s + \omega_i^2}, \quad \zeta_i = \frac{\delta\omega_i}{\omega_i}, \quad K_i = \pm 2\zeta_i \Delta f_i, \tag{23}$$

where the first order TF $H^1$ modeled the contribution of high frequency MEM's with eigenfrequencies higher than $\omega_N$ and is used to adjust the static response, $\zeta_i$ relates to $Q_{mi}$ as $Q_{mi} = 0.5/\zeta_i$. For the FPT in this study, $K_0$ is a negative small value about 1 Hz/V. The time constant $\tau$ corresponds typically to a cut-off frequency of -1 kHz. The other parameters: $\delta\omega_i$ the half bandwidth, $\omega_i$ the eigen-frequency and $\Delta f_i$ the detuning amplitude are the model parameters. A test of the model described in equations Eq. (23) is given for illustration (Figure 13).

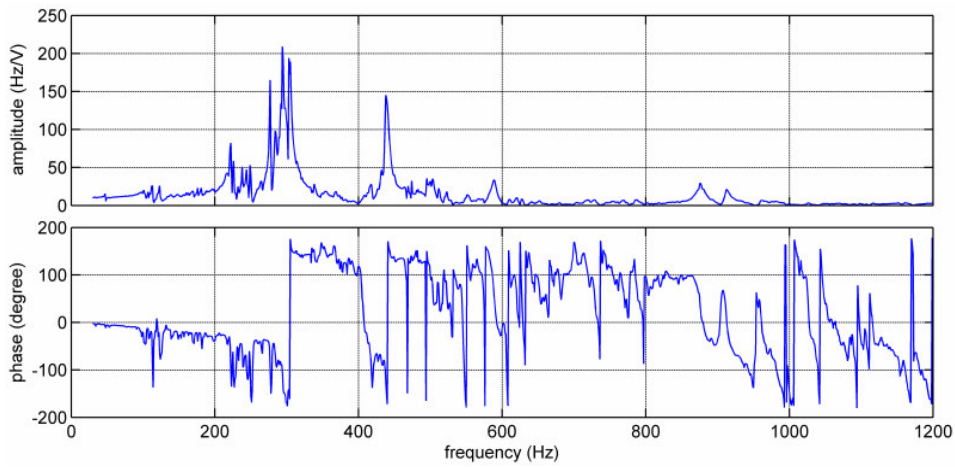


Figure 12: Fast piezoelectric tuner transfer function (measured).

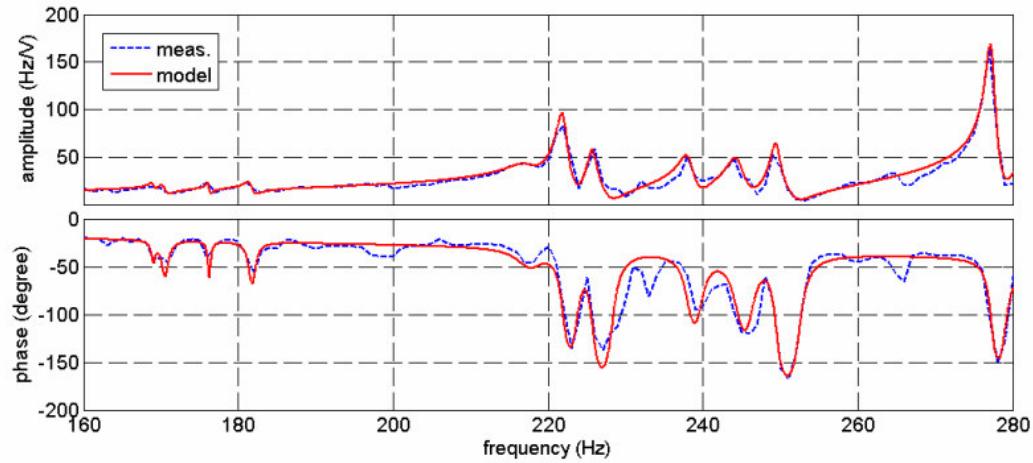


Figure 13: Transfer function model test.

Once the parameters of the model in Eq. (23) are identified with a fit to the measured transfer function, the performance of the detuning compensation may be estimated, regarding the microphonics for instance. Because of the numerous resonances in the transfer function, which limit the loop gain when a tuner is used in a feedback loop, the detuning reduction factor usually restricts itself to 3 or 4 in practice. Another limitation on the detuning compensation lies in the finite resolution of the fast tuner, which found it origin in the mechanical plays and in the electrical driving signal noise. Feedforward methods provide similar reduction factors [11].

Feedforward method is also used for the compensation of Lorentz force detuning, which turns out to be severe especially in a high gradient pulsed cavity, i.e. the RF power is pulsed. Without compensation, the detuning may rise up to a few hundreds Hertz. Fast tuners resolutions are usually good enough to provide an effective compensation. An example of performance achieved with a piezo tuner is shown in Figure 14. More details are found in [12].

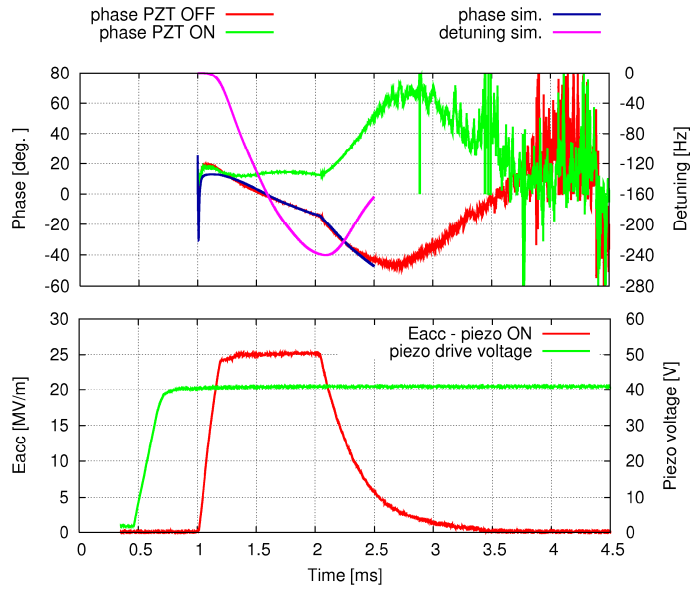


Figure 14: Example of Lorentz force compensation with a fast tuner.

## 3.3 Implementation with Simulink

The numerical solution of the equations given above with Matlab and Simulink does not present majors difficulties except the problem of memory limitation, which require a sequencing of the simulation when many cavities in a linac are addressed. This specificity will be discussed in more details below. For any other aspect of the implementation, readers are asked to refer to the manuals and documentation of the Matlab and Simulink tools. Furthermore, not only one implementation is possible. The choice of the way to implement a numerical solution of the cavity simulation will depend on the experience with the Simulink tool and also on the visual feelings of the scientist since Simulink provides a graphical representation of a system simulation. Figure 15 shows an example of architecture for the cavity simulation, while Figure 16 gives an insight on how the energy gain and phase error equations are implemented.

For the simulation, each bunch is represented by a structure with three fields: charge, energy and phase error. When the bunch repetition frequency is as high as 353.2 MHz, corresponding to a period of about 3 ns, and the frequency of the mechanical eigenmode may be as low as 30 Hz, a simulation for a beam during one mechanical oscillation would require 10 millions bunches. If the linac is composed of 100 cavities, simulation for the bunch energy and phase error after each cavity would correspond to 2 matrices of 1 billion elements, which require a random access memory resource not available on a standard computer. The first step to reduce the memory demand consists in grouping bunches into macro-bunches. The grouping factor by which the charge and repetition period are multiplied is function of the transient beam loading given by Eq. (15). For cavities the parameters of which are similar to the one listed in Table 2, a factor of 10 to 100 may be used without spoiling the simulation accuracy. The transient beam loading would just rise to 50 to 500 V instead of 5 V, still negligible compared to the nominal cavity voltage of 4.413 MV.

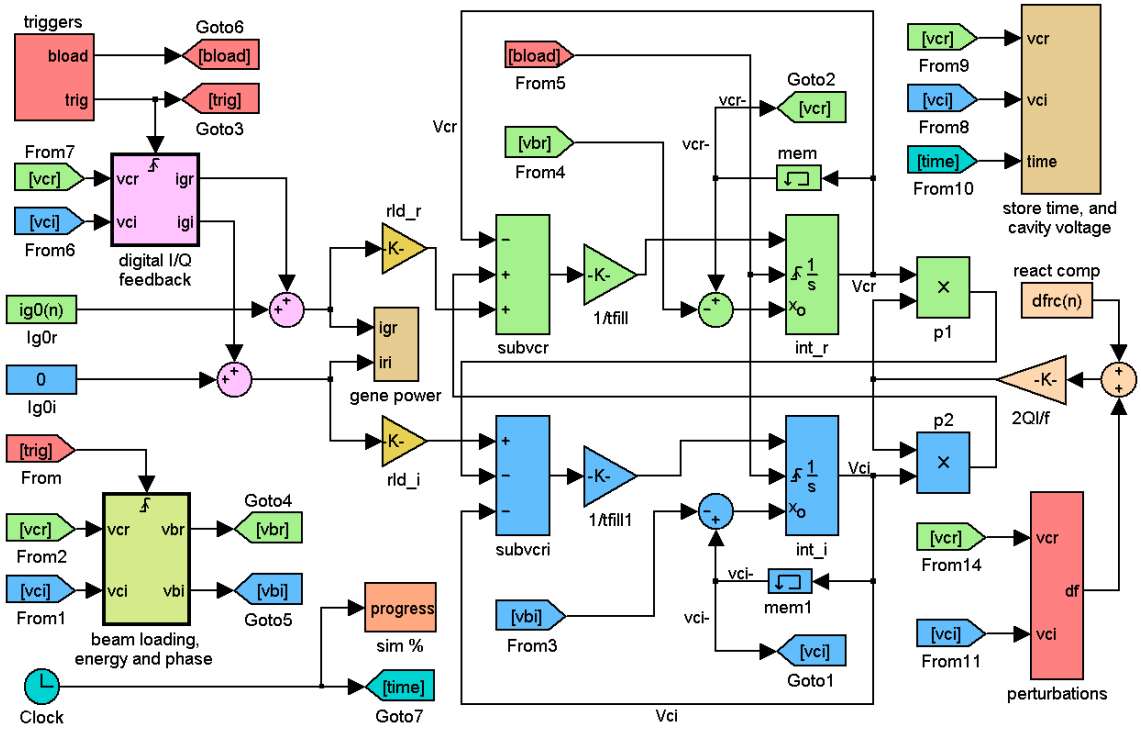


Figure 15: Example of implementation architecture for cavity simulation.

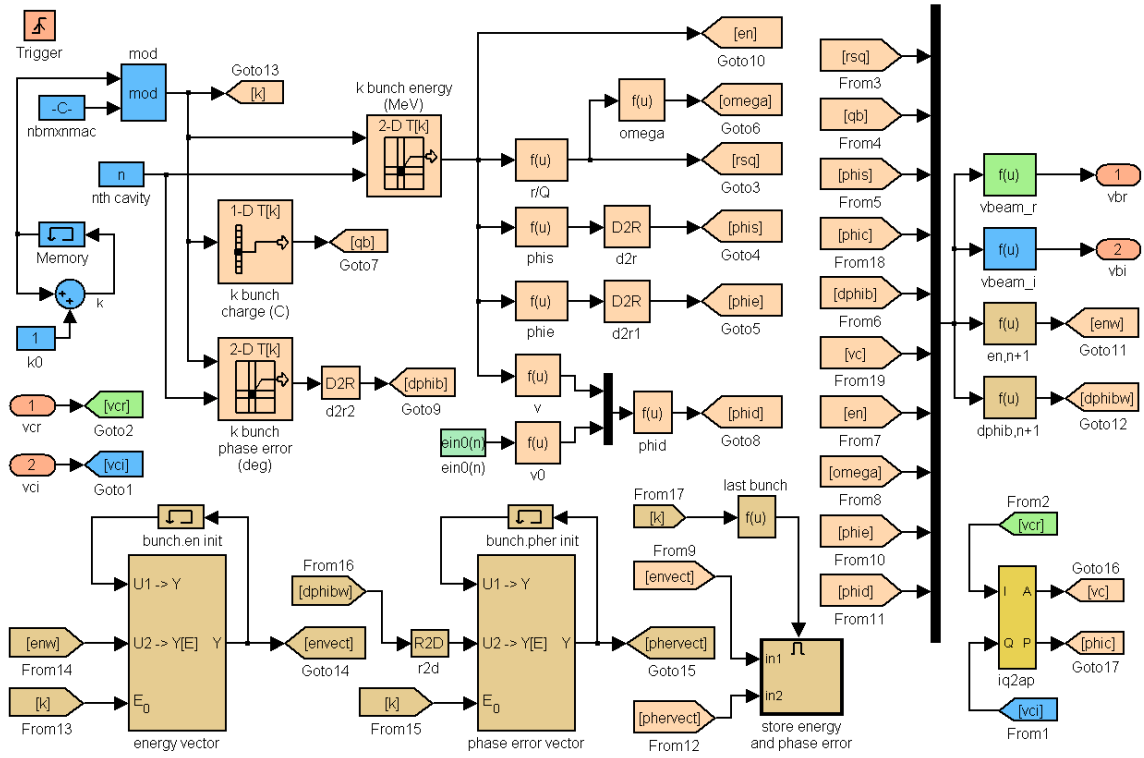


Figure 16: Insight of beam energy and phase computation architecture.

However, this reduction may be insufficient for the memory capability of many standard computers. In addition to the bunch grouping, a thread by thread simulation is recommended. It consists in a sequencing of the simulation. A thread is defined as a succession of a multiple number of a macro-pulse, periodic pattern of the beam. In the case of ADS linac, a macro-pulse would be composed of a number of bunches with the nominal charge and a much smaller number of bunches with reduced charges called gaps, which are dedicated to monitoring measurements. Practically, a simulation is carried out for one thread on the linac first cavity. Once all the macro-bunches haves crossed the cavity, the simulation is stopped. The beam energy and phase errors at the entrance of the next cavity are obtained and the simulation can start for the second cavity. This process is repeated step by step until the last cavity is reached and another thread follows the same treatment. This way, the memory requirement can be alleviated by dividing the beam into small threads.

A difficulty associated to the method lies on the necessity to store the state of a cavity in order to resume the simulation from one thread to the next. The cavity state means all the variables produced at the end of the simulation and the value of which must be considered as initial value to the next simulation. Fundamentally, the cavity voltage (real and imaginary components) and the FIFO registers used in the feedback loop delays emulation have to be saved. But, when Lorentz force detuning is taken into account using a second order model as shown in Eq. (21) or any sub-system modeling involves transfer function block or differential equation, additional integrator blocks are automatically set up. All the integrators blocks state must be saved then. This is done by checking the option “Save to workspace/Final state” of the “Configuration Parameters” panel in the Simulink. This final state can be resumed while checking the “Load from workspace/Initial state” option on the same panel. The structure automatically generated by Simulink has an arrangement, which can be displayed in the workspace as follow:

```
>> final_state
final_state =
       time: []
    signals: [1x123 struct]
>> final_state.signals
ans =
1x123 struct array with fields:
    values
    dimensions
    label
    blockName
    inReferencedModel.
```

A delay modeling is essential in feedback loops because delays have a direct limitation on the maximum gain allowed by the stability of the system and the higher the gain, the better the loop performance. Simulink provides a general transport delay block suitable for that purpose in a single shot simulation. Unfortunately, the content of the FIFO register is not stored in the final state. Therefore, a custom-made delay function should be implemented. One example of implementation is given below (Figure 17):

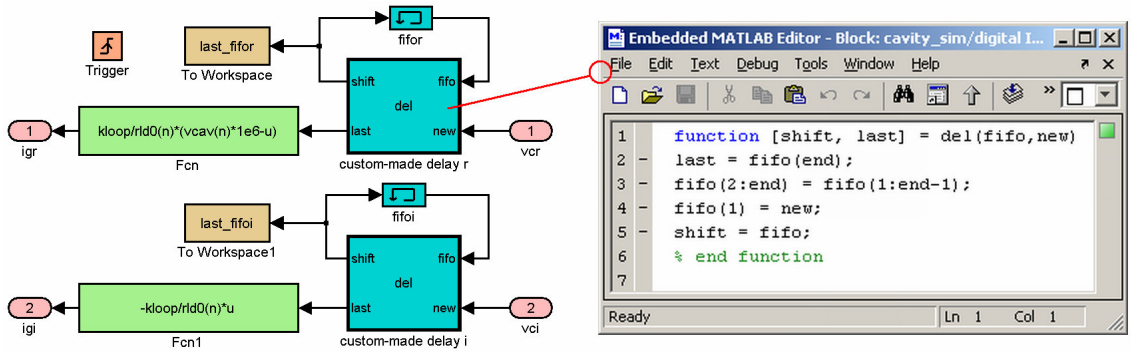


Figure 17: Basic feedback loop with custom-made delays.

The main implementation difficulties for a seamless sequential simulation by threads with Simulink are presented in this section. Thanks to the flexibility and the user-friendly interface of Simulink, many others hardware features of an RF control system may be easily modeled and implemented. For example, the feedback loop shown in Figure 17 is a very basic one, corresponding to Eq.(13), but sampling and digitizing functions may be implemented in a very straightforward way using the standard function blocks of Simulink.

# 4 EXAMPLES OF SIMULATION

This section presents several simulations that serve as an illustration of the kinds of result they can provide. While separating the diverse perturbations, the simulations also help to understand and feel the effect of each other on the beam properties. They may be considered as a general road map in the simulation of an RF control system. However, they do not intend to provide a longitudinal stability analysis of any ADS linac, which is out of the scope of the present report, even through the simulation model proposed here allow such an analysis. This analysis may be carried out in the framework of another Eurotrans deliverable. Unless otherwise stated, simulations results will be given in the steady regime, i.e. at about $5\tau$ as

defined in Eq. (11), which corresponds to about 12 ms and a grouping factor of 50 is considered. Others specific parameters will be listed in each case.

## 4.1 Reference simulation

This simulation is dedicated to validate the code implementation and estimate the accuracy of the numerical solutions. The nominal behaviour of the cavity is simulation with parameters given in Table 2, without perturbation and feedback.

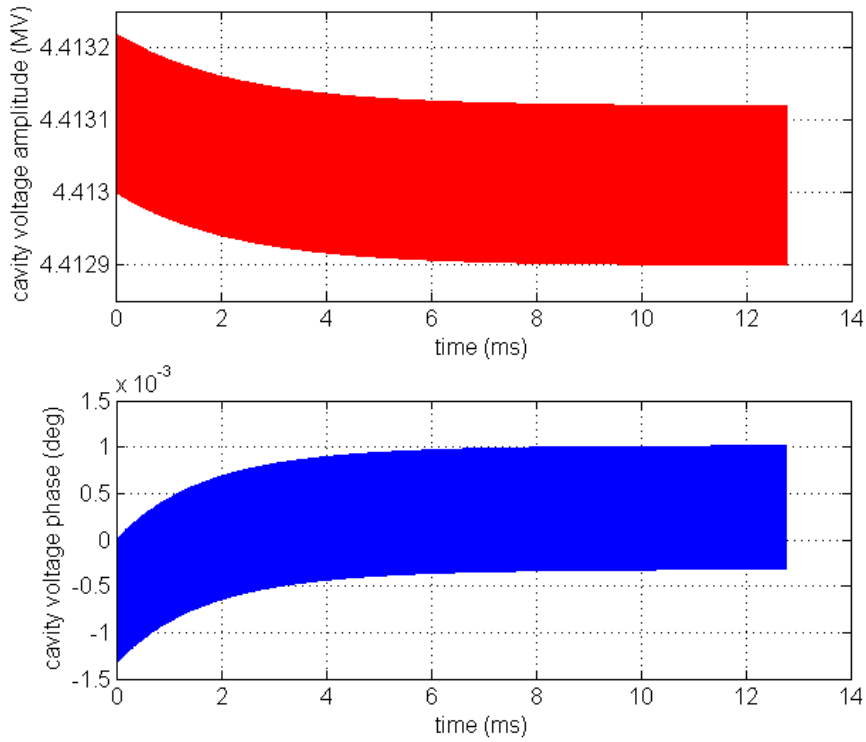


Figure 18: Cavity voltage, amplitude and phase.

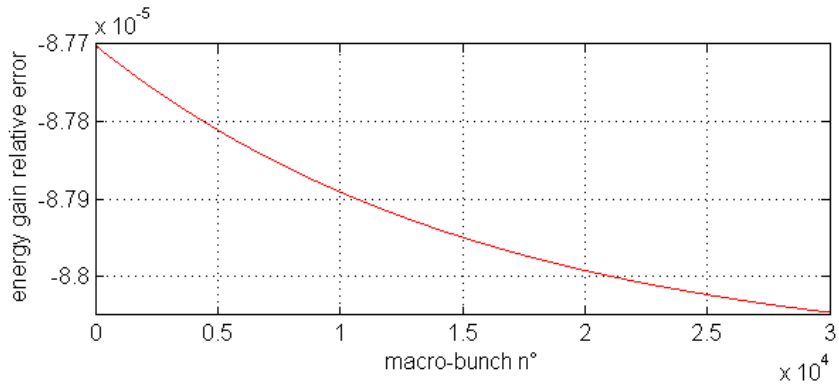


Figure 19: Energy gain relative error.

Figure 18 shows that cavity amplitude and phase computation accuracy are good enough even with a grouping factor of 50. The static and peak to peak errors can be reduced with a reduction the grouping factor. The energy gain error (Figure 19) is directly related here to the cavity amplitude and phase errors. It is also negligible compared to the deviations that are generated by other perturbations as observed in the next sections.

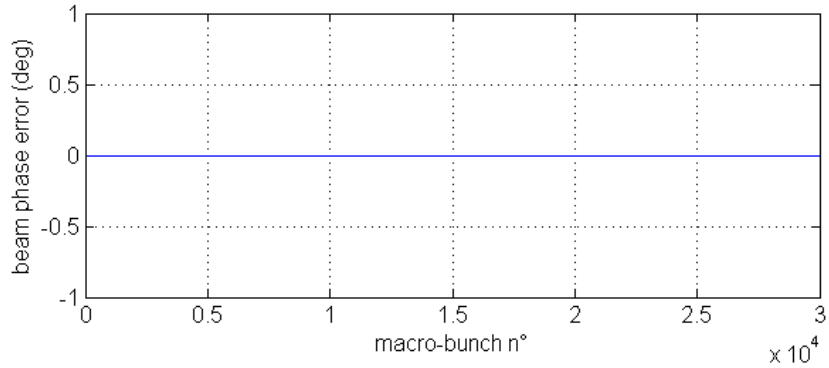


Figure 20: Beam phase error at the cavity exit.

## 4.2 Effect of a gap on the beam, without feedback

Because of the need for nuclear measurements on the target, regular gaps with reduced current or zero current should be arranged in the beam. A typical gap of about 140 µs is considered in the simulation with 50% of current reduction and a duty cycle of 90% for the nominal current. Even if the reactive compensation detuning angle can be corrected for the mean current on the macro-pulse, the beam loading change during a gap appears clearly in the absence of a feedback control. Three threads of 3 macro-pulses are simulated. Cavity voltage amplitude and phase are displayed from the beginning of the simulation (Figure 21) while energy gain error is reported only for the last thread (Figure 22).

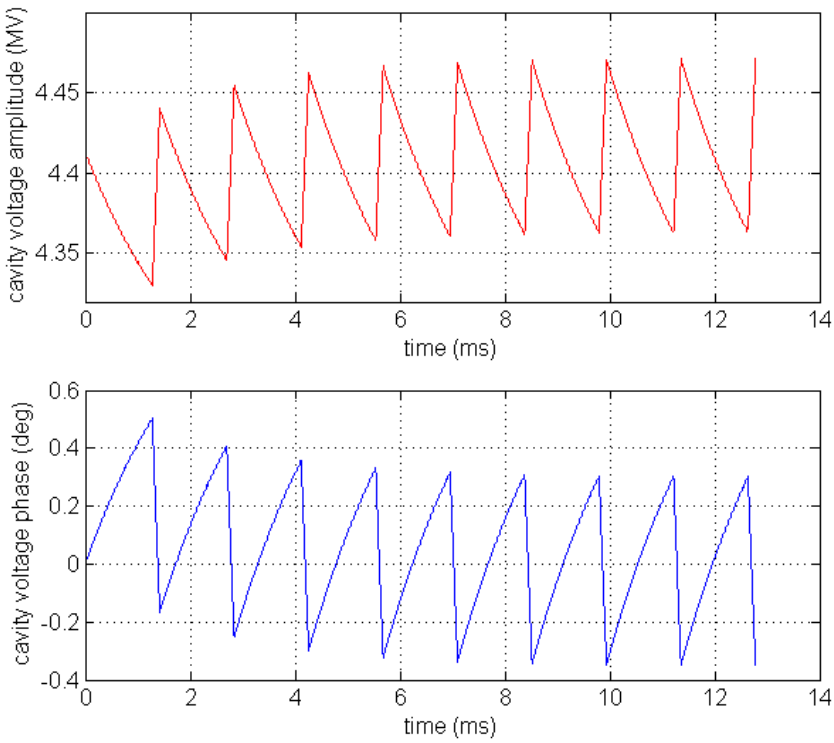


Figure 21: Effect of beam gap on cavity voltage without feedback.

A variation of about 2% is observed on the cavity voltage amplitude. It reflected in about 2% of energy spread (Figure 22) on the beam at the cavity exit. From equations Eq. (16), it

can be seen that the beam phase is not affected by the gaps; a zero phase error like in Figure 20 would be obtained if displayed. In reality, a cavity voltage amplitude variation is always accompanied by a beam phase shift. However, this variation is low enough to be neglected in the simulation. Otherwise, a first order expansion of the beam phase to the energy gain deviation may be used, similarly to Eq. (8). The correction factor would be -2.1°/MeV and the phase shift would be limited to 0.17° peak to peak. To take into account the effect of a gain error to the beam phase, the equation in Eq. (16) can be modified accordingly, denoting $\Delta\xi$ the energy gain:

$$\begin{aligned}
\Delta\phi_b^{n+1,k} &= \Delta\phi_b^{n,k} + \phi_e^{n,k} + \phi_d^{n,k}, \\
\phi_e^{n,k} &= \frac{\partial}{\partial\xi}\left(\phi_e^n\right)_{\xi_0^n}\left(\xi^{n,k} - \xi_0^n\right) + \frac{\partial}{\partial\Delta\xi}\left(\phi_e^n\right)_{\Delta\xi_0^n}\left(\Delta\xi^{n,k} - \Delta\xi_0^n\right), \\
\Delta\xi^{n,k} &= \xi^{n+1,k} - \xi^{n,k}.
\end{aligned} \tag{24}$$

This effect is included for the next simulations. With beam gaps, the beam phase deviation is given in Figure 23.

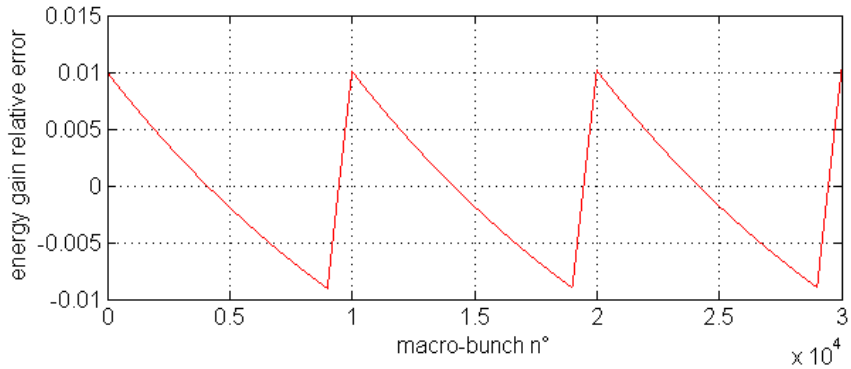


Figure 22: Energy gain deviation on the last thread due to beam gaps.

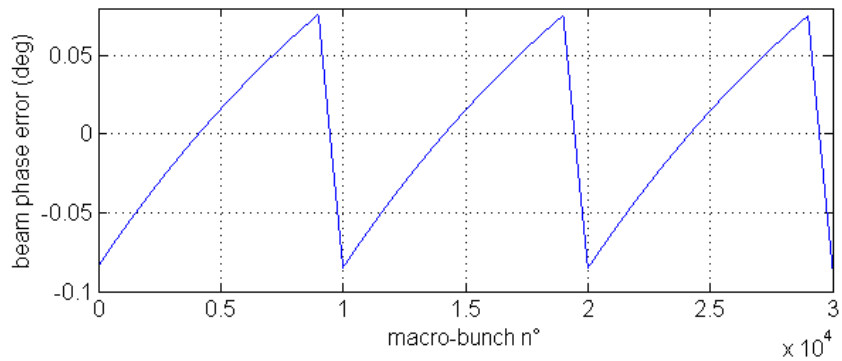


Figure 23: Beam phase deviation on the last thread due to beam gaps.

## 4.3 Static injection energy error

As mentioned in Section 2.4, the energy gain and phase slippage in a cavity is very sensitive to the injection energy. For a 1 MeV positive injection error, the results are shown in Figure 24, Figure 25 and Figure 26. An energy gain error of about 26% is observed without feedback.

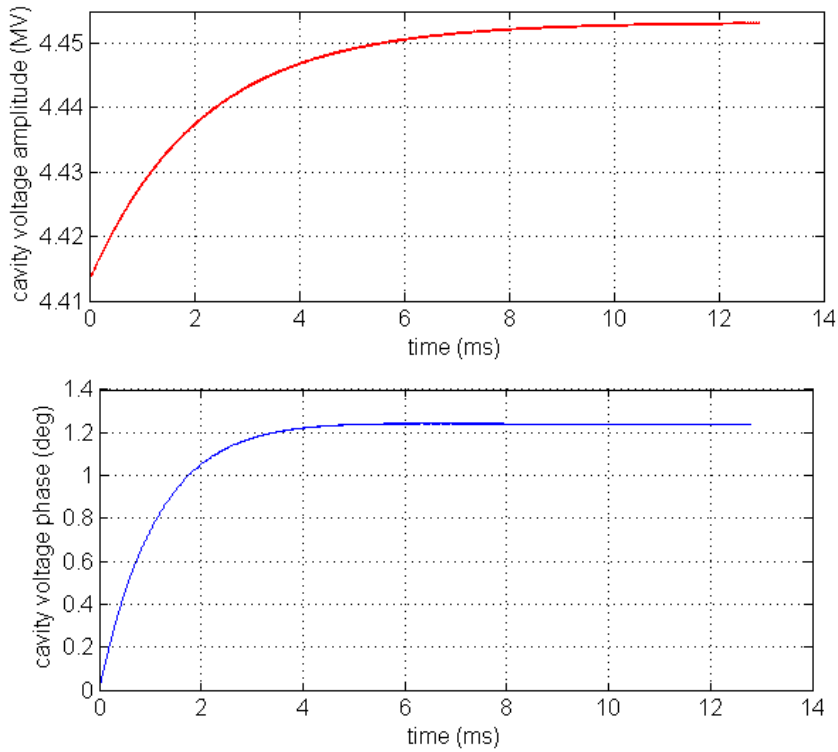


Figure 24: Effect of an injection energy error on the cavity voltage without feedback.

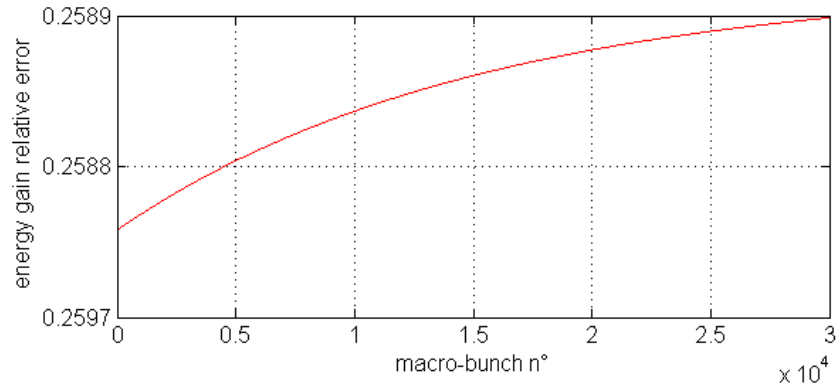


Figure 25: Energy gain error due to injection energy error without feedback.

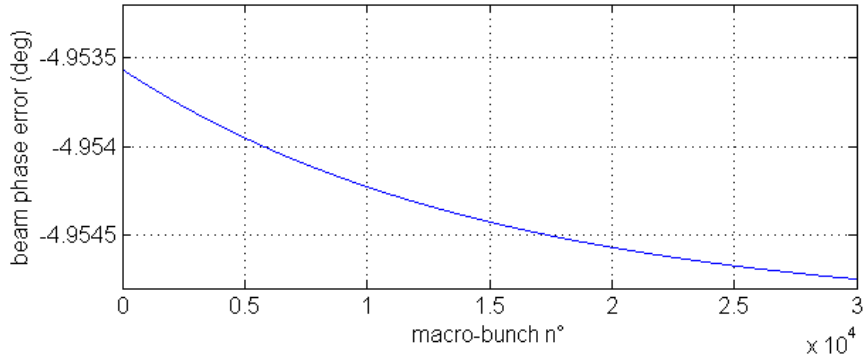


Figure 26: Beam phase deviation due to injection energy error without feedback.

A feedback RF control system would ensure that all the bunches get the same energy gain and phase shift, but the offset error due to the static injection error is hardly reduced (Figure 30, Figure 31 and Figure 32). An open gain of 100 and a delay of 2 µs were considered in the feedback control.

## 4.4 Microphonics perturbation

In order to assess the effect of a harmonic detuning of the cavity due to the microphonics, a detuning amplitude of 50 Hz with a modulation frequency of 250 Hz are used in the simulation, which is carried out over 24 ms because of the pretty slow modulation. Results are displayed in Figure 27, Figure 28 and Figure 29.

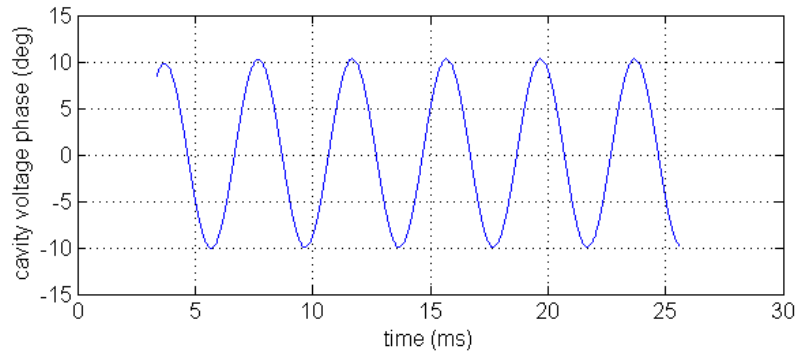


Figure 27: Cavity voltage phase under a simple microphonic perturbation.

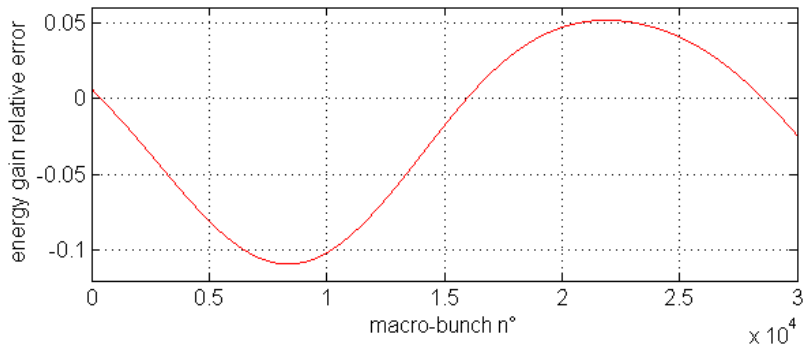


Figure 28: Energy gain error due to a microphonic perturbation.

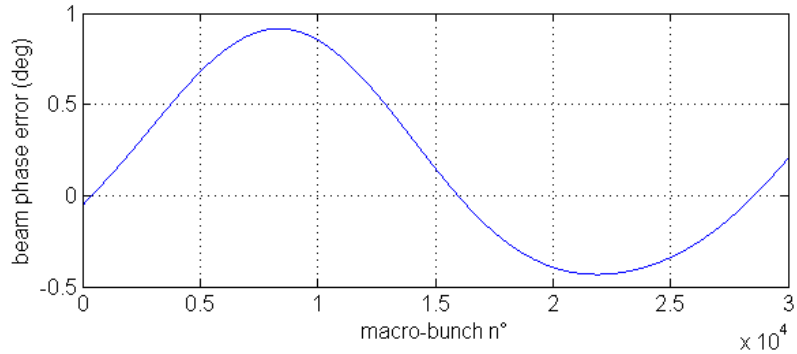


Figure 29: Microphonics induced beam phase error.

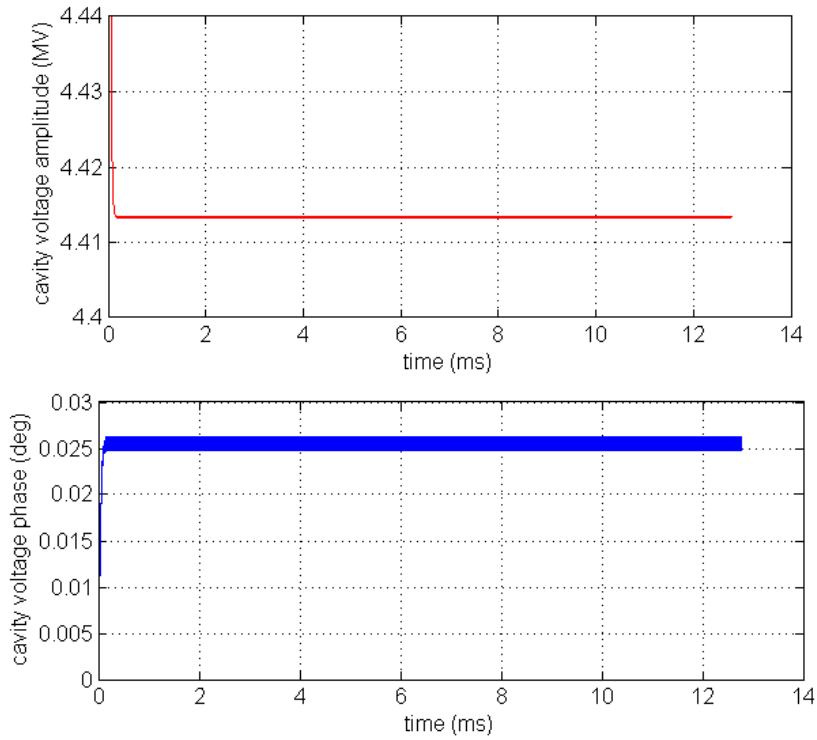


Figure 30: Effect of an injection energy error on the cavity voltage with feedback.

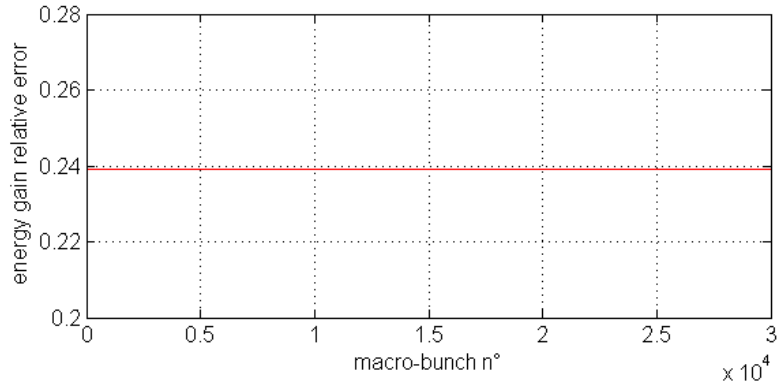


Figure 31: Energy gain error due to injection energy error with feedback.

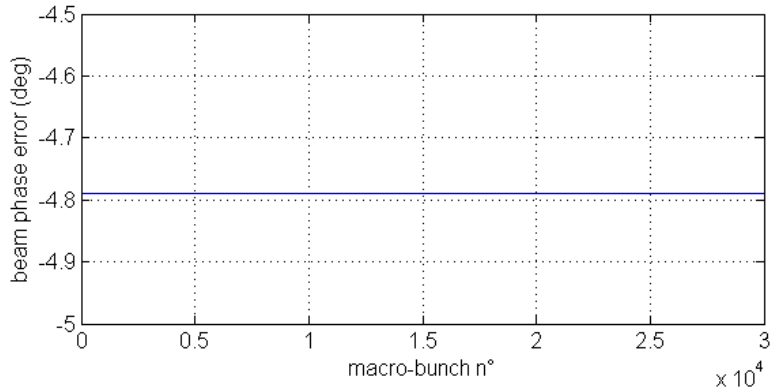


Figure 32: Beam phase deviation due to injection energy error with feedback.

## 4.5 Lorentz force perturbation

A realistic simulation of Lorentz force perturbation requires a careful analysis of each mechanical mode as suggested in Section 3.2, which is out of the scope of this report. Instead, the following simulation just intends to illustrate the ponderomotive resonance that may be a concern for ADS cavities because of the gap with reduced beam loading. If the frequency of gap repetition (or one of its harmonics) matches the eigenfrequency of one mechanical mode with significant $k_m$ sensitivity as it appear in Eq. (21), an oscillation of the cavity resonant frequency is excited whose amplitude scales proportionally to $k_m$ and $Q_m$. This effect is evidenced in a simulation with a single mechanical mode at 352.2 Hz, with a Lorentz detuning sensitivity of -0.2 Hz/(MV/m)$^2$ and a mechanical quality factor of 50. For this simulation, the bunch grouping factor is set to 100 in order to speed up the solution and minimize the memory requirement. A macro-pulse of 10 000 macro-bunches with a half current 10% gap is used. Consequently, the gap pattern repetition matches exactly to 352.2 Hz. The simulation is first performed without feedback (Figure 33, Figure 34 and Figure 35).

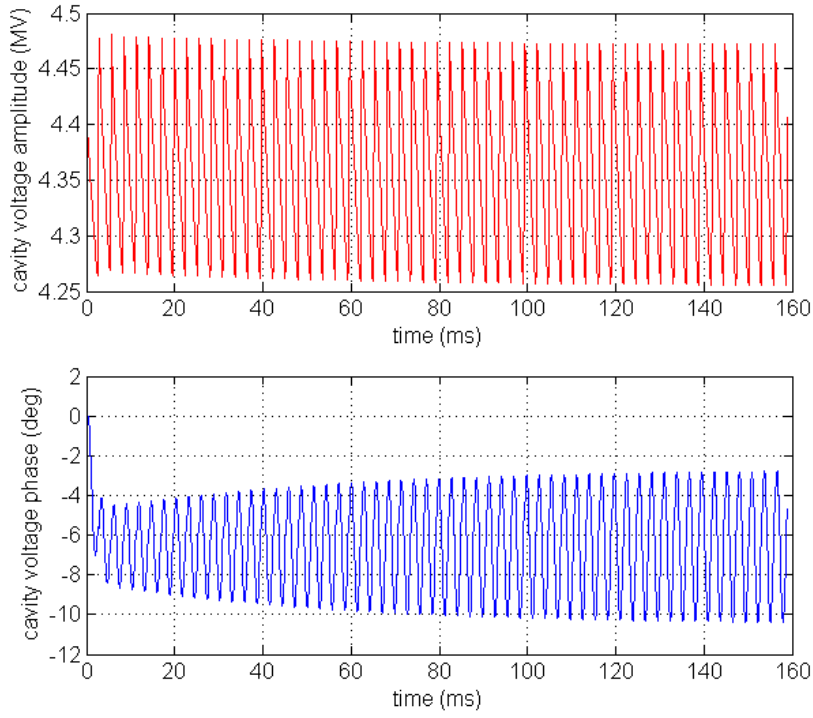


Figure 33: Cavity voltage due to a single mechanical mode excited by the Lorentz force.

It can be noticed that the Lorentz force always tend to lower the resonant frequency of an elliptical cavity. As a result the cavity phase shifts to a negative value (Figure 33). Since the nominal synchronous phase is also negative, the term of cosine function is reduced. This explains why the energy gain error presents a negative offset of about 8% with a 6% modulation due to the resonance. Since the beam gets a lower energy gain, the beam phase shifts to a positive value, meaning that the bunches lag behind the nominal reference bunch. This phenomenon appears more clearly while comparing the oscillations in Figure 34 and Figure 35.

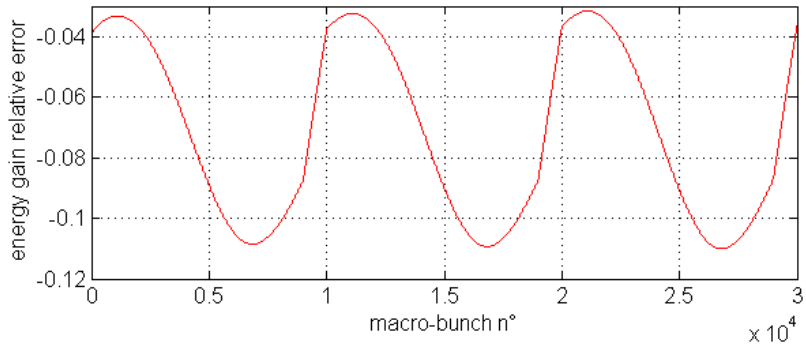


Figure 34: Gain error due to the Lorentz force.

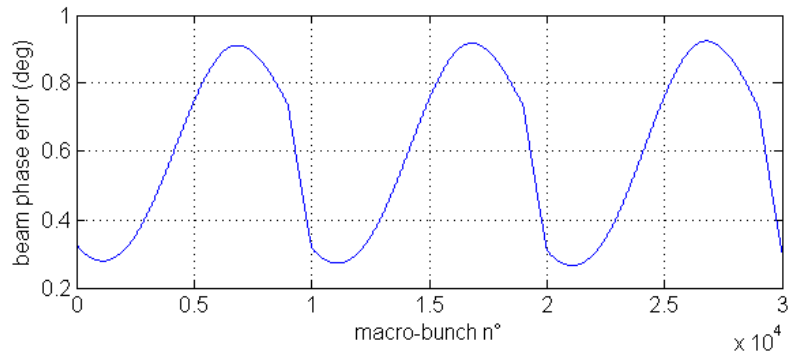


Figure 35: Beam phase deviation due to Lorentz force.

## 4.6 Gaps, microphonics, Lorentz force detuning and feedback

The different simulation above have shown that all the perturbation sources, should it be gaps, microphonics or Lorentz force detuning may easily produce an energy gain error higher than 1%. The last example of simulation combines all these perturbations (however without injection energy error) in a system where a feedback loop with the same parameters than the one already considered in Section 4.3 is implemented.

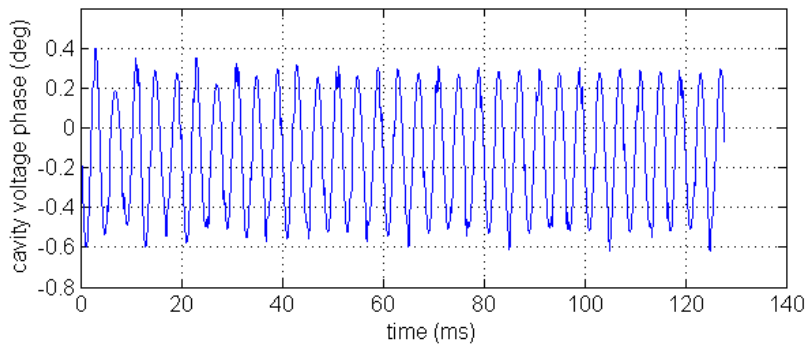


Figure 36: Cavity voltage phase compensation of perturbation with feedback.

In this example, the feedback action succeeded to keep the relative energy gain error below 1% (Figure 37). The cavity and beam phase deviations are respectively limited to 1 and 0.1 degree peak-peak. However the perturbation of the beam gaps still appears clearly (Figure

37 and Figure 38) even under the compensation of the feedback loop. When the beam current drops, resulting in a reduction of beam loading, the cavity voltage amplitude tends to climb to a higher value if the RF source power is kept identical, leading to a slightly higher gain (Figure 37). With a feedback loop activated, the tendency is rapidly but not instantaneously, because of delays and bandwidth limitation, counteracted by a reduction of the generator power.

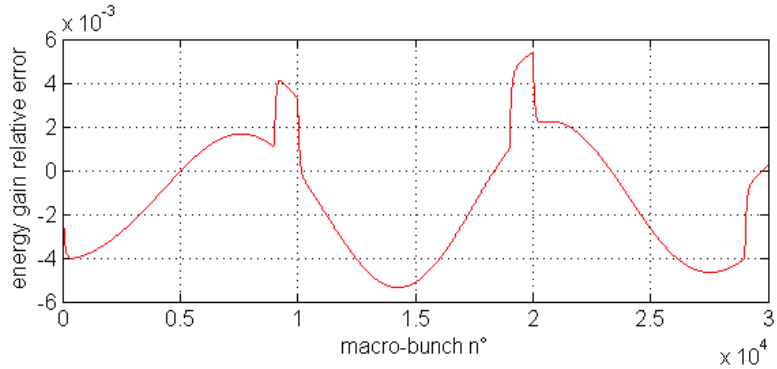


Figure 37: Residual energy gain error with feedback.

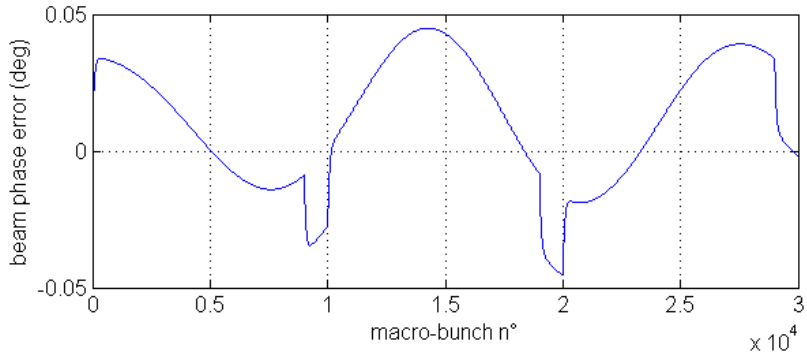


Figure 38: Residual beam phase error with feedback.

The efficiency of the feedback loop in the cavity detuning compensation should be paid with an increase of the generator power. Practically, an extra power budget of about 10 to 20 % is needed for the feedback compensation. With the assumptions made on the microphonics and Lorentz force detuning, the peak power takes more than 25% of the nominal value (Figure 39).

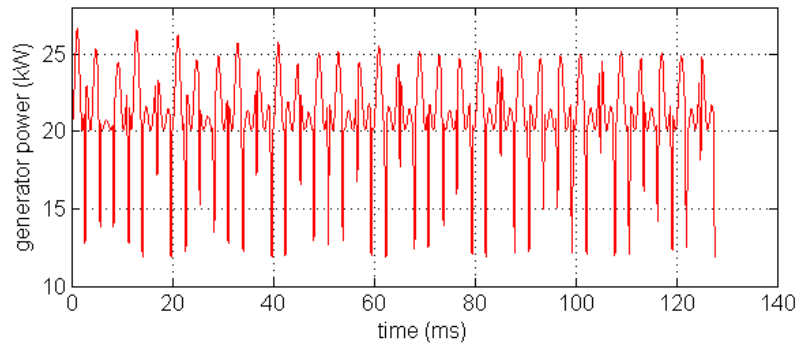


Figure 39: Generator power for feedback compensation.

# 5 CONCLUSION

The acceleration of non relativistic particles, with a velocity lower than the light velocity, in an RF cavity is more complex than for relativistic particles, i.e. electrons at energy higher than a few megaelectron-volts. Non-linear behaviours appear because of the phase slippage inside the cavity. However, in the perspective the RF control system modeling and simulation, which deal with small excursions of the cavity voltage amplitude and phase, a first order expansion approach may be adopted. The computation of the necessary parameter derivatives is obtained numerically using a trajectory tracking code, which fully accounts for the phase slippage. Combining the first order approximation to the usual equivalent circuit representation of the beam to cavity interaction, a set of equations is produced in order to perform a bunch by bunch simulation along a linac. Furthermore, a sequential algorithm compatible with a minimum memory usage is recommended for long time analysis of an RF control system over a large linac. Typically perturbations are also presented with their possible modeling. Finally, some simulation examples are provided as a guideline for the use of this modeling and simulation approach.

# 6 REFERENCES

[1] J-L. Biarrotte et al., « Preliminary RF Control Specifications », Eurotrans Project, deliverable D1.17, November 2005

[2] Matlab is a high-level language for intensive numerical computation and Simulink is a Matlab toolbox for system simulation with a graphical interface: http://www.mathworks.com/.

[3] P. B. Wilson, « High Energy Electron Linacs: Applications to Storage Ring RF Systems and Linear Colliders », SLAC-PUB-2884, July 1981

[4] G. Devanz, private communication

[5] I. M. Kapchinskiy, « Theory of Resonance Linear Accelerators », Harwood Academic Publishers, 1985

[6] J.M. Tessier, Ph D dissertation, « Stabilisation de Champ dans des Cavités Supraconductrices en Régime Pulsé », Université Paris XI, 1996

[7] T. Shilcher, Ph D dissertation, « Vector Sum Control of Pulsed Accelerating Fields in Lorentz Force detuned Superconducting Cavities », Universität Hambourg, 1998

[8] F. Orsini, Ph D dissertation, « Phénomènes d'Instabilités et de Résonances crées par un Système HF dans un Anneau », Université Paris VI, 1999

[9] M. Luong et al., « Analysis of Microphonics Disturbances and Simulation for Feedback Compensation », Proceedings of EPAC 2006, Edinburgh, Scotland, 2006

[10] G. Devanz et al., « Numerical Simulations of Dynamic Lorentz Detuning of SC Cavities », Proceedings of EPAC 2002, Paris, France, 2002

[11] A. Neumann et al., « Characterization of a Piezo-based Microphonics Compensation System at HoBiCaT », Proceedings of EPAC 2006, Edinburgh, Scotland, 2006

[12] G. Devanz et al., « Active Compensation of Lorentz Force Detuning of a TTF 9-cell Cavity in Cryholab », Proceedings of LINAC 2006, Knoxville, Tennessee USA, 2006